Chemical Geology 495 (2018) 18–26

Contents lists available at ScienceDirect

Chemical Geology

journal homepage: www.elsevier.com/locate/chemgeo

# Triple oxygen isotope mass balance for the Earth's oceans with application to Archean cherts☆

Sukanya Sengupta*, Andreas Pack

*Georg-August-Universität, Geowissenschaftliches Zentrum, Abteilung Isotopengeologie, Goldschmidtstraße 1, 37077 Göttingen, Germany*

ARTICLE INFO

Editor: Michael E. B

*Keywords:*
Triple oxygen isotopes
Seawater $\delta^{18}O$
Cherts
Mass balance model

ABSTRACT

The oxygen isotope composition of the Earth's oceans is buffered by high- and low-T exchange with the lithosphere. We present a triple oxygen isotope mass balance model for the Earth's oceans. The model is based on triple oxygen isotope measurements of rocks from various reservoirs including high- and low-T alteration products. The modern ocean water composition can be well-matched if the ratio between continental weathering and high-T seafloor alteration is ~25% higher than previously assumed. The mass balance suggests that putative Precambrian low-$\delta^{18}O$ ocean water would fall on a trend with slope $\lambda = 0.51$ passing through "modern" ice-free-world seawater. Exemplified application to a published Phanerozoic and Archean chert data suggest precipitation in cool oceans with modern-like $\delta^{18}O$ followed by diagenetic alteration with involvement of meteoric water.

## 1. Introduction

### 1.1. The ocean oxygen isotope buffer

The presence of the Earth's oceans, in the sense of liquid surface water, can be traced back to the Archean (Nutman et al., 1996, 1997) and possibly the Hadean (Peck et al., 2001; Wilde et al., 2001) era. The high $\delta^{18}O$ values (for definition of the δ-notation, see McKinney et al., 1950) of Hadean zircon has been used as evidence that oceans formed as early as 4.4 Ga ago (Wilde et al., 2001). The oldest water-lain sediments on Earth date back to > 3.85 Ga (Nutman et al., 1997). As liquid water is one prerequisite for the development of life, physico-chemical condition of the early oceans is of great interest.

The oxygen isotope composition of modern oceans is close to $\delta^{17}O \approx \delta^{18}O \approx 0‰$. Seawater is not in isotopic equilibrium with the lithosphere. Instead, it was shown by Muehlenbachs and Clayton (1976) that the isotope composition of seawater is in steady-state, buffered by low- and high-T exchange with the lithosphere. Low-T alteration of rocks is counterbalanced by a decrease of the $\delta^{18}O$, whereas high-T alteration leads to a decrease of the $\delta^{18}O$ of the hydrosphere, respectively.

It has been observed that the $\delta^{18}O$ of Archean marine chemical sediments (carbonates, cherts, phosphates) is ~15‰ lower when compared to the composition of modern counterparts (Degens and Epstein, 1962; Perry, 1967; Longinelli and Nuti, 1968; Knauth and Epstein, 1976; Veizer and Hoefs, 1976; Shemesh et al., 1983; Veizer et al., 1999; Knauth, 2005).

Three causes for the low $\delta^{18}O$ have been discussed in the literature: *i*) Higher ocean temperatures were suggested by Knauth and Epstein (1976) and others (Knauth and Lowe, 1978, 2003; Shemesh et al., 1983, 1988; Karhu and Epstein, 1986; Jean-Baptiste et al., 1997; Muehlenbachs, 1998; Knauth, 2005; Robert and Chaussidon, 2006; Blake et al., 2010; Marin et al., 2010; Tartèse et al., 2017; Garcia et al., 2017). Temperatures of as high as 80°C (with ocean water with a $\delta^{18}O \approx 0‰$) would lead to formation of chemical sediments with $\delta^{18}O$ lower than their modern "cool" counterparts, *ii*) lower $\delta^{18}O$ values of Archean seawater were first suggested by Perry (1967) and other authors (Veizer et al., 1999; Wallmann, 2001; Kasting et al., 2006; Jaffrés et al., 2007; Shields, 2007). A lower $\delta^{18}O$ of seawater (down to −14‰, Jaffrés et al., 2007) is explained by a higher ratio of low-T to high-T alteration processes. A reduced oxygen flux from high-T alteration has been proposed for mid-ocean ridge crests in shallow water resulting in earlier boiling and less effective interaction with the oceanic crust (Kasting et al., 2006), and *iii*) diagenesis is known to lower the $\delta^{18}O$ of chemical sediments, such as carbonates (e.g., Banner and Hanson, 1990). The low $\delta^{18}O$ values of ancient chemical sediments hence may be explained by interaction with low- $\delta^{18}O$ meteoric water and/or interaction with seawater at higher, diagenetic temperatures. This idea

☆ Declarations of conflicting interests: none.

* Corresponding author.
*E-mail address:* sukanya.sengupta@geo.uni-goettingen.de (S. Sengupta).

https://doi.org/10.1016/j.chemgeo.2018.07.012
Received 18 May 2018; Received in revised form 7 July 2018; Accepted 9 July 2018
Available online 03 August 2018

was first formulated by Degens and Epstein (1962).

No consensus has yet been reached on why Archean chemical sediments are isotopically so different from the modern counterparts.

We suggest that triple oxygen isotope measurements of chemical sediments can provide insights into the cause for the low $\delta^{18}O$ values. Pioneering work by Barkan and Luz (2005) and Luz and Barkan (2011) on high-precision measurements of $\delta^{17}O$ and $\delta^{18}O$ of terrestrial water showed that small deviations from the correlation between $\delta^{17}O$ and $\delta^{18}O$ provide interesting additional information about processes in the Earth hydrosphere. Pack and Herwartz (2014, 2015) first showed that deviations from the correlation between $\delta^{17}O$ and $\delta^{18}O$ are also present in the Earth lithosphere. They suggested that these deviations were caused by purely mass-dependent processes, namely the interaction between the hydrosphere and lithosphere at different temperatures. Herwartz et al. (2015) presented a first application and demonstrated that high-precision triple oxygen isotope measurements can give unique insights into the history of rocks, namely their exchange with the hydrosphere (see also the recent work by Bindeman et al., 2018). Sharp et al. (2016) presented the first empirical calibration of the triple oxygen isotope fractionation between silica and water and demonstrated that the triple isotope fractionation exponent θ is, indeed, a function of temperature as predicted by theory (Matsuhisa et al., 1978; Young et al., 2002; Cao and Liu, 2011).

Here we present a new mass balance model for ocean water that is based on high-precision triple isotope data of reservoirs that interact with the hydrosphere. We demonstrate that high-precision triple isotope analyses of Archean chemical sediments provide information about the composition of ancient ocean water.

## 2. Materials and methods

### 2.1. Sampling

In order to model the effect on both, $\delta^{17}O$ and $\delta^{18}O$ of the hydrosphere-lithosphere exchange, we analyzed the triple oxygen isotope composition of low- and high-T altered rocks from oceanic and continental settings. Sample names and sample descriptions are listed in Table 1.

### 2.2. Oxygen isotope analyses

Samples were analyzed by means of laser fluorination (with $BrF_5$ as oxidation agent; see Sharp, 1990) in combination with gas chromatography and dual-inlet gas source mass spectrometry (for details, see Pack et al., 2016). Bulk rock samples with hydrous phases were reacted in Ni tubes following the protocol described by Clayton and Mayeda (1963). The oxygen that was liberated by reaction with $BrF_5$ was then purified and analyzed using the same extraction line that we use for the laser fluorination. The external reproducibility was tested on San Carlos olivine (laser fluorination) and Dörentrup quartz (Ni tubes; Fiebig et al., 1999; Pack and Herwartz, 2014) to ± 0.5‰ for $\delta^{18}O$ and ± 0.01‰ for $\Delta'^{17}O$ (1σ, SD). The $\delta^{17}O$ and $\delta^{18}O$ values are reported relative to VSMOW2 scale.

In order to display small variations in the $\delta^{17}O/\delta^{18}O$ ratios, the $\Delta'^{17}O$ has been introduced. Here, we use $\Delta'^{17}O$ relative to a reference line (RL) with slope 0.5305 and zero intercept (Eq. (1)).

$$\Delta'^{17}O^{\text{sample}}_{\lambda_{RL}=0.5305} = 10^3 \cdot \ln\left(\frac{\delta^{17}O^{\text{sample}}_{VSMOW2}}{10^3} + 1\right) - 0.5305 \cdot 10^3 \cdot \ln\left(\frac{\delta^{18}O^{\text{sample}}_{VSMOW2}}{10^3} + 1\right) \quad (1)$$

where necessary, literature $\delta^{17}O$ values were recalculated relative to San Carlos olivine with a $\Delta'^{17}O$ value of −0.06‰ (mean San Carlos $\Delta'^{17}O$ value from Pack et al., 2016, and Sharp et al., 2016). The fractionation in $^{17}O/^{16}O$ and $^{18}O/^{16}O$ between phases (e.g., for equilibrium fractionation) or reservoirs (e.g., for a kinetic process) A and B is related through the triple isotope fractionation exponent θ (Eq. (2)).

$$\ln\left(\frac{\delta^{17}O^{A}_{VSMOW2} + 1000}{\delta^{17}O^{B}_{VSMOW2} + 1000}\right) = \theta_{A-B} \cdot \ln\left(\frac{\delta^{18}O^{A}_{VSMOW2} + 1000}{\delta^{18}O^{B}_{VSMOW2} + 1000}\right) \quad (2)$$

For distinct physical processes (e.g., equilibrium or kinetic fractionation between 2 phases or reservoirs), we use the θ. For the slope of the reference line (Eq. (1)) or trends in the 3-isotope space that cannot be reduced to distinct fractionation processes, we use the symbol λ. A trend with slope λ can be result of a number of different equilibrium and/or kinetic fractionation processes.

## 3. Results

The results of triple oxygen isotope measurements are listed in Table 2.

## 4. The mass balance model

Our triple isotope mass balance model is based on the model by Muehlenbachs (1998). The steady-state $\delta^{17}O$ and $\delta^{18}O$ of seawater is calculated according to the isotopic fluxes of $^{16}O$, $^{17}O$ and $^{18}O$ to and from the oceans via water/rock interaction. Five major geological processes *j* are considered to control the total oxygen budget of the oceans via lithosphere-hydrosphere interactions (Fig. 1):

i) continental weathering (*cw*)
ii) high-T ocean floor alteration (*sp*)
iii) low-T ocean basalt alteration (*sfw*)
iv) continental growth (*cg*), and
v) mantle recycling (*r*).

The mass balance equation considers the fluxes, the changes in $\delta^{17}O$ and $\delta^{18}O$ during water/rock interaction, and the reservoir size (Eq. (3)).

$$\frac{\partial}{\partial t}\delta^{18}O^{\text{Ocean}} = \sum \frac{F^i_j}{m_{\text{Ocean}}} \times \Delta(\delta^{18}O_j) \quad (3)$$

with:

$$\Delta(\delta^{18}O_j) = \delta^{18}O^{\text{unaltered}}_j - \delta^{18}O^{\text{altered}}_j \quad (4)$$

For the model equations we shall define a $\Delta^{17}O$ here with:

$$\Delta^{17}O = \delta^{17}O - 0.5305 \times \delta^{18}O \quad (5)$$

Note that this $\Delta^{17}O$ is not calculated from the linearized δ notation, but from the δ notation as defined by McKinney et al. (1950). We use the $\Delta^{17}O$ here (and not $\Delta'^{17}O$; Eq. (1)) because it is mass conservative with $\Delta^{17}O^{\text{bulk}} = \Sigma X_i \Delta^{17}O^i$. The shift in $\delta^{17}O$ is now calculated from the shift in $\delta^{18}O$ and the shift of the rock in $\Delta^{17}O$ during the exchange process with:

$$\Delta(\delta^{17}O_j) = 0.5305 \times \Delta(\delta^{18}O^{\text{unaltered}}_j) + \Delta(\Delta^{17}O^{\text{unaltered}}_j) \quad (6)$$

and:

$$\Delta(\Delta^{17}O_j) = \Delta^{17}O^{\text{unaltered}}_j - \Delta^{17}O^{\text{altered}}_j \quad (7)$$

with:

$$\frac{\partial}{\partial t}\delta^{17}O^{\text{Ocean}} = \sum \frac{F^i_j}{m_{\text{Ocean}}} \times \Delta(\delta^{17}O_j) \quad (8)$$

Continental weathering (*cw*) is the most important flux modifying the composition of the hydrosphere. The flux $F_{cw}$ is adopted from Muehlenbachs (1998). Continental weathering lowers the $\delta^{18}O$ of oceans. Unaltered igneous rocks and granitoids have $\delta^{18}O$ values in the range of 6 to 10‰ (Taylor, 1978). For the unaltered continental crust, we adopt $\delta^{18}O$ = 7‰ (Muehlenbachs, 1998) and a $\Delta'^{17}O$ = −0.060‰

**Table 1**
List of samples with locality and description.

| Sample | Sample description |
|---|---|
| Altered oceanic crust samples, Low-T, from IODP Hole U1383C | The low-T altered oceanic crust samples are from IODP Hole U1383C (22°48.1241′ N; 46°03.1662′ W), situated at 4414 m water depth, North Pond area of the North Atlantic Ocean. The North Pond (23°N, 56°W) is a 8 km × 15 km isolated sediment pond on the western flank of the mid-Atlantic ridge in an ~8 Ma crust (Orcutt et al., 2013). The lithology within this borehole below 164 mbsf, where our samples hail from, comprises glassy to variolitic to cryptocrystalline basalts (mostly pillow flows) with variable degrees of low temperature alteration or seafloor weathering. All sample descriptions are from IODP Preliminary Reports (Expedition 336 Scientists, 2012). |
| OC-LT-1 | Aphyric to sparsely/moderately phyric pillow lava from Core 13R1, Section 1, depth 173.82 mbsf, within Sub-unit 3–6, interval 109–112 cm. Average vein width is ~0.2 mm (0.6 mm maximum) with mainly grayish brown halos (~11 mm average width). Vein filling is 25% smectite, 25% carbonate, 25% FeOx/iddingsite, 25% zeolite. Chilled margins with variable extents of palagonitization (~50%) with reddish brown to light green alteration are seen. Massive gray basalt with plagioclase phenocrysts generally develop brown alteration halos are present along exposed veins. Based on visual estimates, sample is about 10% altered. |
| OC-LT-2 | Aphyric pillow lava from Core 31R, Section 2, 313.99 mbsf depth, within Lithologic unit 3–28, interval 45–49 cm. Veins of average and maximum width ~0.3 mm with dark to grayish brown halos are present within the pillows. The vein fillings include 20% smectite, 40% carbonate, 20% FeOx/iddingsite and 20% zeolites (from IODP core descriptions).The degree of overall alteration in this sample, based on visual estimation, is about 20%. |
| OC-LT-3 | Sample from Core 32R, Section 3, at a depth of 324.31 mbsf within Lithologic unit 3–29, interval 1–4 cm. This unit is not well described in the IODP core description logs. It may be a breccia/pseudobreccia. The sample is very heavily altered, ~80% from visual estimates. |
| Altered oceanic crust samples, High-T, from DSDP/ODP Hole 504B | The high-T altered oceanic crust samples are from Leg 83 of DSDP/ODP Hole 504B (01°13.63′ N; 83°43′0.81′ W) located 200 km south of the Costa Rica Rift spreading centre in the east equatorial Pacific. Our samples come from depths of ~1090 to 1350 m – the region of upper sheeted dolerite dikes complex (SDC) (the SDC extends from 1055 to > 2111 mbsf) within a 6 Ma old oceanic crust. The upper SDC (down to 1500 mbsf) is variably altered to the Greenschist facies. Alteration is highly heterogeneous and most intense along cm-sized chlorite ± actinolite veins. Sample descriptions are from Alt et al., 1996 and Bach et al., 2003. |
| OC-HT-1 | Chilled margin breccia from Core 141R of Hole 504B, Section 1, Piece 7, Litho zone SDC, Litho type B, retrieved from a depth of 1350.3 mbsf, interval 50–57 cm. The sample is completely chloritized and contains very fine grained rock fragments. Voids and vein fillings include cement of prehnite, chlorite, and anhydrite. Based on visual estimates this sample has been described as 100% altered. |
| OC-HT-2 | Diabase breccia from Core 122R of Hole 504B, Section 1, Piece 7, Litho zone SDC, Litho type B, depth 1214.3 mbsf, interval 76–85 cm. The olivine in the sample is completely chloritized, the plagioclase heavily altered to chlorite, albite and quartz. The clinopyroxene is heavily altered to chlorite and actinolite. The matrix of the rock is completely chloritized. The extent of alteration, from visual estimates, is 80%. |
| Pal-1 | Palagonite sample collected during the MERIAN cruise MSM3 in 2014 to the North Pond Area, western flank of Mid-Atlantic Ridge (see more details about the North Pond in sample description of low-T altered oceanic crust samples). The sample Pal-1 was recovered during Dive J2-772 (on 9.4.2014) from core 2A, 3749 water depth, from basement outcrops just northwest of the sediment pond. The location of the dive is 22°49.224′ N, 46°09.680′ W. It belongs to a lava roof slab that has a strongly palagonitized thick glass crust on the upper side and thin glass on lower side. It's been exposed to oxidizing seawater throughout. Age of the sample is ~8 Ma. Sample description has been taken mainly from personal communications with Wolfgang Bach (Professor, University of Bremen, Bremen, Germany), who was a petrologist aboard the MSM37 cruise, and from cruise report Maria S. Merian-Berichte (Villinger, 2014). |
| Sha-1 | Medium to fine grained, finely laminate, dark gray coloured oil shale of Lower Jurassic age (Lias lithostratigraphic group of Europe, i.e., 200 to 180 Ma) from the Posidonia Shale formation (“Posidonienschiefer”), Wenzen Hills, Lower Saxony, Germany. Shales intercalated with bituminous limestones (Bottjer et al., 2001) within the formation. These shales are postulated to have been deposited in an anoxic (or nearly anoxic) deep water environment on the seafloor of the Paleo-Tethys Ocean. The rock contains 40 wt% carbonate. It was donated by Alex Gehler (Geowissenschaftliches Zentrum, Göttingen, Germany). |

(adopted from a compilation of published continental crust data; see Fig. 2). The unaltered metamorphic crust is assumed to have $\delta^{18}O = 12‰$ (Muehlenbachs, 1998) and $\Delta'^{17}O = -0.078‰$ (also adopted from a compilation of published continental crust data; see Fig. 2). As approximation for the continental weathering endmember, we analyzed the silicate fraction of a Liassic shale (Table 1). This is reflective of detrital input from the continents. Our measured $\delta^{18}O = 16.1‰$ is close to Muehlenbachs's (1998) adopted value of 17‰. The corresponding $\Delta'^{17}O$ value is measured to −0.173‰, falling within the field of crustal materials (Fig. 2). A set of shales has recently been reported by Bindeman et al. (2018). The Phanerozoic shales measured by them is close in $\delta^{18}O$ to 17‰ (between 15and 19‰) and have a range of $\Delta'^{17}O$ values from −0.093 to −0.227‰. For our study we adopt our measured value of −0.173‰ for the continental weathering end member.

The second most important flux is high-T seafloor alteration (*sp*; Fig. 1). Its absolute value is the largest but a small $\Delta(\delta^{18}O_{sp})$ and $\Delta(\delta^{17}O_{sp})$ prevents it from being the most important flux in the model. At high temperatures, equilibration between ocean water and oceanic crust leads to altered crust with $\delta^{18}O < 5.6‰$. Our samples OC-HT-1 and OC-HT-2 both have a $\delta^{18}O < 5.6‰$ (Table 2) and reflect exchange with ocean water at high temperatures and high water/rock ratios (Fig. 3).

The sample OC-HT-1 is used as approximation for an entirely high-T altered endmember. The $\Delta'^{17}O$ of high-T altered crust shifted up by ~0.05‰ to −0.019‰ and reflects the high-T equilibration with seawater ($\Delta'^{17}O^{sw} = -0.005‰$). The θ value for the water/rock equilibration at 300–350 °C (temperature estimate from Alt et al., 1986, and Kawahata et al., 1987) is calculated to 0.5273 (Fig. 5), which is well within the range of high-T fractionation in rocks (Pack and Herwartz, 2014). Sample OC-HT-2 is a ~50% partially altered oceanic crust sample and falls on a mixing line between unaltered oceanic crust (represented by MORB) and the altered endmember OC-HT-1 (Fig. 5).

Low-T alteration of oceanic crust (*sfw*) leads to the formation of hydrous rocks with $\delta^{18}O > 5.6‰$. Samples OC-LT-1, OC-LT-2, and OC-LT-3 all have elevated $\delta^{18}O$ and fall on a trend between highly-altered palagonite Pal-1 and unaltered oceanic crust represented by MORB (Fig. 4).

The $\delta^{18}O$ value of palagonite Pal-1 is ~16‰ and likely does not represent the low-T altered endmember, which would be a clay with $\delta^{18}O$ of ~25‰ (Sheppard and Gilg, 1996), but is higher than the most altered oceanic crust sample analyzed by (Muehlenbachs and Clayton,

**Table 2**
Triple oxygen isotope data of samples analyzed for the mass balance model. Throughout the text and in tables the $\delta^{17}O$ and $\delta^{18}O$ values are reported on the VSMOW2 scale and the unit is "per mil" (‰). Also listed are the fractionation factors α for the fractionation in $^{17}O/^{16}O$ and $^{18}O/^{16}O$ between samples $O_2$ and reference bottle $O_2$. For $\delta^{17}O$ and $\delta^{18}O$ we give 3 digits of precision here in order to facilitate calculation of $\Delta'^{17}O$ in a different reference frame.

| Sample | Method | $1000\ln(\alpha^{17/16}_{S.-R.})$ | $1000\ln(\alpha^{18/16}_{S.-R.})$ | $\delta^{17}O$ | $\delta^{18}O$ | $\Delta^{17}O$ | $\Delta'^{17}O$ |
|---|---|---|---|---|---|---|---|
| OC-LT-1 | Ni reactor | −1.210 | −2.826 | 4.817 | 9.255 | −0.093 | −0.082 |
| | | −2.166 | −4.641 | 3.857 | 7.425 | −0.082 | −0.075 |
| | | −1.857 | −4.079 | 4.167 | 7.991 | −0.072 | −0.064 |
| | | −2.171 | −4.649 | 3.852 | 7.416 | −0.082 | −0.075 |
| | | −1.867 | −4.054 | 4.157 | 8.016 | −0.096 | −0.087 |
| *Mean* | | | | *4.2* | *8.0* | *−0.085* | *−0.077* |
| *2σ(SEM)* | | | | *0.4* | *0.7* | *0.009* | *0.008* |
| OC-LT-2 | Ni reactor | −0.945 | −2.325 | 5.083 | 9.761 | −0.095 | −0.083 |
| | | −1.616 | −3.605 | 4.409 | 8.469 | −0.084 | −0.074 |
| | | −1.274 | −2.935 | 4.753 | 9.145 | −0.098 | −0.088 |
| | | −1.065 | −2.552 | 4.963 | 9.531 | −0.093 | −0.082 |
| *Mean* | | | | *4.8* | *9.2* | *−0.093* | *−0.082* |
| *2σ(SEM)* | | | | *0.3* | *0.6* | *0.006* | *0.005* |
| OC-LT-3 | Ni reactor | 0.241 | −0.010 | 6.276 | 12.101 | −0.143 | −0.124 |
| | | 0.045 | −0.446 | 6.079 | 11.660 | −0.106 | −0.089 |
| | | 0.867 | 1.159 | 6.906 | 13.285 | −0.142 | −0.119 |
| | | 0.597 | 0.614 | 6.634 | 12.732 | −0.120 | −0.100 |
| | | 1.470 | 2.226 | 7.513 | 14.366 | −0.108 | −0.082 |
| | | −0.073 | −0.696 | 5.960 | 11.407 | −0.091 | −0.075 |
| | | −0.209 | −0.916 | 5.823 | 11.185 | −0.110 | −0.094 |
| | | −0.331 | −1.128 | 5.701 | 10.970 | −0.119 | −0.103 |
| *Mean* | | | | *6.4* | *12.2* | *−0.117* | *−0.098* |
| *2σ(SEM)* | | | | *0.4* | *0.8* | *0.013* | *0.012* |
| OC-HT-1 | Ni reactor | −3.666 | −7.580 | 2.352 | 4.468 | −0.018 | −0.015 |
| | | −3.570 | −7.387 | 2.448 | 4.662 | −0.025 | −0.022 |
| | | −3.675 | −7.587 | 2.344 | 4.461 | −0.023 | −0.020 |
| *Mean* | | | | *2.4* | *4.5* | *−0.022* | *−0.019* |
| *2σ(SEM)* | | | | *0.06* | *0.11* | *0.004* | *0.004* |
| OC-HT-2 | Ni reactor | −3.358 | −6.964 | 2.660 | 5.087 | −0.038 | −0.035 |
| *2σ(SD)* | | | | *0.5* | *1.0* | *0.020* | *0.020* |
| Pal-1 | IR laser | | | | | | |
| | Step-wise fluorination | | | | | | |
| | Step1, 70% | 3.189 | 5.572 | 9.247 | 17.766 | −0.178 | −0.138 |
| | Step2, 17% | 0.445 | 0.288 | 6.481 | 12.402 | −0.099 | −0.079 |
| | Step3, 13% | −1.146 | −2.706 | 4.882 | 9.376 | −0.092 | −0.081 |
| *Mean (according to yield)* | | | | *8.199* | *15.744* | *−0.153* | *−0.122* |
| *2σ(SEM)* | | | | *0.3* | *0.6* | *0.012* | *0.012* |
| Sha-1 (silicate portion) | IR laser | 1.954 | 3.291 | 8.001 | 15.447 | −0.194 | −0.163 |
| | | 2.425 | 4.214 | 8.476 | 16.385 | −0.216 | −0.181 |
| | | 2.453 | 4.253 | 8.504 | 16.425 | −0.210 | −0.175 |
| *Mean* | | | | *8.3* | *16.1* | *−0.206* | *−0.173* |
| *2σ(SEM)* | | | | *0.3* | *0.6* | *0.012* | *0.012* |

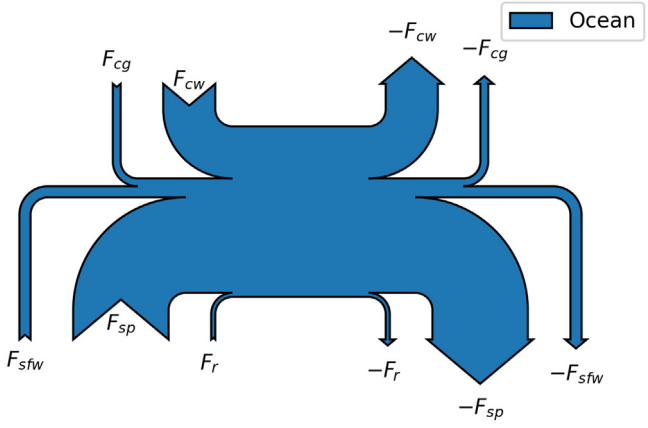


**Fig. 1.** Illustration of the oxygen mass balance with approximate relative flux sizes indicated. Fluxes F for low-T (*sfw*) and high-T (*sp*) sea floor alteration, continental weathering (*cw*), continental growth (*cg*), and mantle recycling (*r*) are indicated.

1972). Our data show that an increase in $\delta^{18}O$ goes along with a decrease in $\Delta'^{17}O$ from initially −0.06‰ to −0.122‰ (Table 2, Fig. 5) due to low-T $\theta < 0.5305$ (see Sharp et al., 2016, for the silica-water low-T equilibrium). We extrapolate the trend through the partially altered oceanic crust samples and the palagonite to $\delta^{18}O = 25‰$ (Sheppard and Gilg, 1996), which gives the putative clay endmember with an extrapolated $\Delta'^{17}O = -0.147 \pm 0.015‰$ (Fig. 5).

The flux $F_{cg}$ for continental growth is taken from (Muehlenbachs, 1998). Newly formed crust is a mixture of 90% oceanic crust and 10% sediments. So, we need to know the oxygen isotope composition of deep sea sediments that have a contribution to the final composition of newly accreted crust. We assume a value of 26‰ for deep sea sediments $\delta^{18}O$, as estimated by Muehlenbachs (1998). For the $\Delta'^{17}O$ of deep sea sediments a value of −0.145‰ is adopted based on the low-T silica-water fractionation data presented in Sharp et al. (2016).

Mantle recycling *r* also influences the steady-state composition of the hydrosphere. The flux $F_r$ is taken from Muehlenbachs (1998). Recycling of water into the mantle leads to an increase in $\delta^{18}O$ as the water is eventually reset to a more mantle like $\delta^{18}O$ value. For the mass balance, we divide the bulk subducted crust in three components: *i*) low-T altered oceanic crust, *ii*) high-T altered oceanic crust, and *iii*) unaltered fresh oceanic crust. Based on the fluxes $F_{sfw}$ and $F_{sp}$ adopted in this study 1.8 $km^3$ and 15$km^3$ of oceanic crust suffers low- and high-T alteration annually, respectively. The amount of new oceanic crust created each year is assumed to be 25 $km^3$. The average $\delta^{18}O$ values of the three components is taken as 12‰ (low-T altered crust), 4‰ (high-

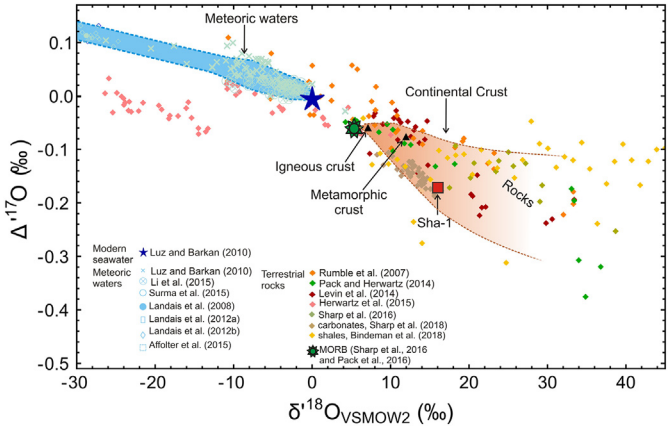


**Fig. 2.** A $\Delta'^{17}O$ vs. $\delta'^{18}O$ compilation of literature data on modern seawater (Luz and Barkan, 2010, dark blue star), meteoric water (Luz and Barkan, 2010, Li et al., 2015, Surma et al., 2015, Landais et al., 2008, Landais et al., 2012a, Landais et al., 2012b, Affolter et al., 2015; light blue symbols), MORB (mantle $\Delta'^{17}O$ from Pack et al., 2016, and Sharp et al., 2016; green complex star) and various terrestrial rocks (Rumble et al., 2007, Pack and Herwartz, 2014, Levin et al., 2014, Herwartz et al., 2015, Sharp et al., 2016 and 2018, Bindeman et al., 2018; diamonds). This figure has been used to estimate the average $\delta^{17}O$ compositions of igneous and metamorphic rocks for the model corresponding to $\delta^{18}O$ values of 7‰ and 17‰ respectively. The analysis of a Liassic shale from this study (Sha-1) is also displayed. (For interpretation of the references to colour in this figure legend, the reader is referred to the web version of this article.)

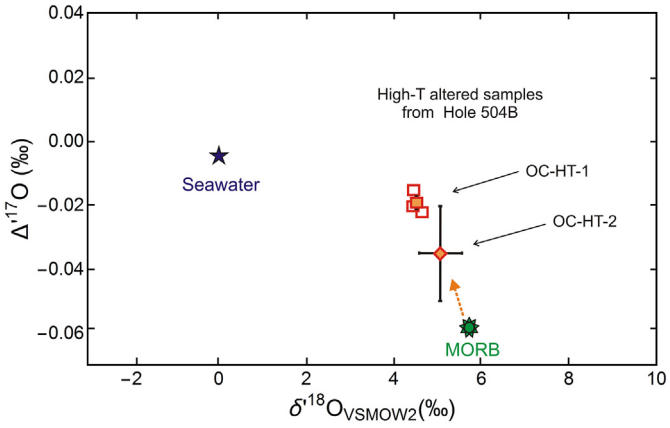


**Fig. 3.** Plot of $\Delta'^{17}O$ vs. $\delta'^{18}O$ of seawater (Luz and Barkan, 2010, blue star), unaltered MORB (green complex star) and two samples of high-T altered oceanic crust from IODP Hole 504B (see Table 1 for sample details). The MORB $\delta^{18}O$ value is from (Muehlenbachs, 1998) and $\Delta'^{17}O$ value is set to −0.060‰ (based on the Earth mantle values from Pack et al., 2016, and Sharp et al., 2016). (For interpretation of the references to colour in this figure legend, the reader is referred to the web version of this article.)

T altered crust) and 5.8‰ (unaltered crust), respectively. Based on the proportions of these components and their $\delta^{18}O$ values, bulk subducted crust has a $\delta^{18}O$ of 5.5‰ (7.2% low-T altered crust, 60% high-T altered crust, and 32.8% unaltered oceanic crust). Considering a 3‰ fractionation between rock and water (taken from Muehlenbachs, 1998), the connate water trapped inside the subducted crustal rocks has a $\delta^{18}O$ of 2.5‰. The $\Delta'^{17}O$ of connate water can be estimated by drawing mixing lines between end members of low- and high-T alteration of oceanic crust and unaltered MORB (Fig. 6). The $\Delta'^{17}O$ of bulk subducted crust is −0.037‰, which is the $\Delta'^{17}O$ at 5.5‰ $\delta^{18}O$ of a mixing curve between low- and high-T alteration end members with 30% unaltered crust. Adopting a θ value of 0.528 between rock and water (using the silica-water fractionation at high-T as approximation; Sharp et al., 2016) the

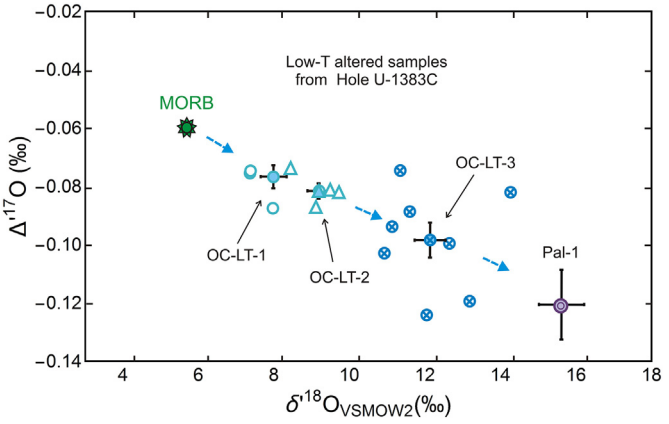


**Fig. 4.** Plot of $\Delta'^{17}O$ vs. $\delta'^{18}O$ of low-T altered oceanic crust samples (OC-LT-1, -2, and -3) from IODP hole U1383C along with unaltered MORB (as representative for fresh oceanic crust; $\Delta'^{17}O = -0.060$‰ (based on the Earth mantle values from Pack et al., 2016, and Sharp et al., 2016) and a palagonite sample Pal-1, which is a low-T alteration product.

connate water $\Delta'^{17}O$ is calculated to be −0.030‰.

The water that leaves the mantle is at high-T equilibrium (> 1000°C) with silicates. Di Rocco and Pack (2015) demonstrated that no fractionation between vapor and silicate melts is observed at 1500°C. Hence, the water that is eventually released from the mantle has a composition identical to the mantle, i.e. $\delta^{18}O = 5.5$‰ and $\Delta'^{17}O = -0.060$‰. The early estimate by Silverman (1951) that water released from the mantle has higher $\delta^{18}O$ is likely due to the early measurements of mafic rocks having $\delta^{18}O \approx 7$‰.

The mass balance model was run according to Eq. (3) and Eq. (8), incorporating all present-day flux magnitudes $F_j$ along with the $\Delta(\delta^{18}O)$ and $\Delta(\delta^{17}O)$ associated with each process. The uncertainty of the model result is calculated using Monte Carlo simulations with uncertainties of all input parameters considered (Tables 2 and 3). Steady state is reached after $2.6 \times 10^8$ years. The steady state result for an ice-free world is $\delta^{18}O^{SW\text{-}IF} = -0.36 \pm 0.5$‰, which is close to the expected value of −1‰ for an ice-free world (e.g., by Shackleton and Kennett, 1975). The steady state $\Delta'^{17}O^{SW\text{-}IF}$ is $= -0.017 \pm 0.015$‰ (SD) and is also close to the expected value of $\Delta'^{17}O^{SW\text{-}IF} = -0.004 \pm 0.003$‰ (Tables 4 and 5).

## 5. Discussion

### 5.1. The mass balance model

The results of the mass balance demonstrate that not only the $\delta^{18}O$, but also the $\Delta'^{17}O$ of seawater (different from most rocks and meteoric waters) can be understood in terms of a steady state between the lithosphere (continental and oceanic crust and mantle) and ocean water. For each process, changes in $\delta^{18}O$ and $\Delta'^{17}O$ have to be known and considered. It is apparent from the mass balance that the model $\delta^{18}O$ is ~0.6‰ higher and the $\Delta'^{17}O$ is 0.013‰ lower than the estimated seawater in an ice-free world. The steady-state composition of the model would come into agreement with the actual seawater composition if the high-T ocean floor alteration flux $F_{sp}$ is by 40% lower or the continental weathering flux $F_{cw}$ is by 75% higher than given in the mass balance model by Muehlenbachs (1998). A 25% lower $F_{sp}$ in combination with a 25% higher $F_{cw}$ (i.e., higher $F_{cw}/F_{sp}$ ratio) would also bring the model ($\delta^{18}O^{SW} = -1.2$‰, $\Delta'^{17}O^{SW} = -0.004$‰) and real-world data in excellent agreement (Tables 4 and 5).

### 5.2. Application to the question of low-$\delta^{18}O$ Precambrian seawater

It has been suggested that the $\delta^{18}O$ of seawater was lower (e.g., by

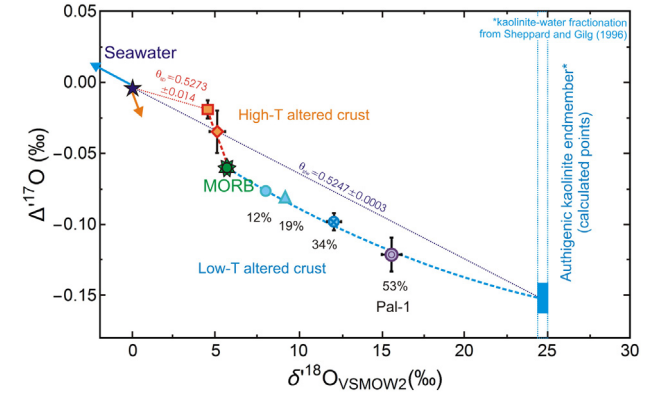


**Fig. 5.** Plot of low and high-T altered oceanic crust samples in $\delta'^{18}O$ vs. $\Delta'^{17}O$ space. The low-T altered samples are marked in blue symbols, whereas the high-T altered samples are marked in orange symbols. The palagonite sample is also a result of low-T alteration of basalts, and is shown in purple double circle. The mean value of each sample is plotted along with the standard errors (SE). Where error bars are not visible, the SE is smaller than the size of the symbol used. The blue dashed curve marks a mixing line between pristine MORB and 100% altered end-member clay (calculated value). The high $\delta^{18}O$ of the clay, a result of low-T alteration, decreases the $\delta^{18}O^{SW}$ and increases the $\Delta'^{17}O^{SW}$, as shown by blue arrow. High-T alteration has the opposite effect; partial alteration increases the $\delta^{18}O^{SW}$ and decreases the $\Delta'^{17}O^{SW}$, whereas a completely altered end-member attains the $\Delta'^{17}O$ value of MORB itself (as shown by orange arrow). (For interpretation of the references to colour in this figure legend, the reader is referred to the web version of this article.)

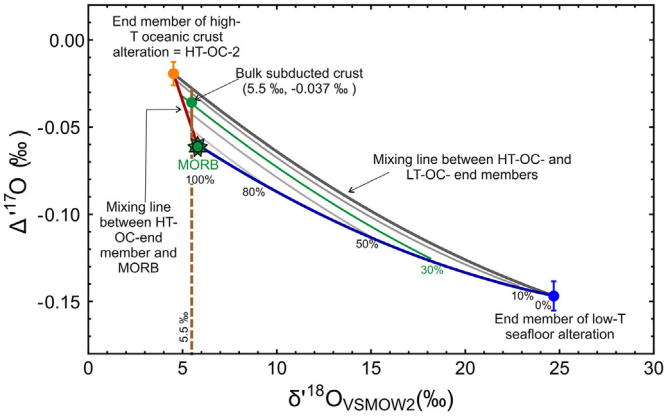


**Fig. 6.** Plot of high and low-T alteration end members (orange and blue dots respectively) and mixing lines between them with variable amounts of unaltered oceanic crust, i.e., MORB (green complex star) (based on values from Pack et al., 2016 and Sharp et al., 2016). The amount of unaltered crust for the different mixing lines is indicated in percentage values. The composition of the bulk subducted crust must fall in the field bounded by the following three mixing curves: LT-end member – MORB, HT- end member – MORB, LT- end member – HT- end member. The green dot represents the bulk subducted crust which lies on the mixing curve with 30% unaltered crust. (For interpretation of the references to colour in this figure legend, the reader is referred to the web version of this article.)

**Table 4**
Real world and modeled triple oxygen isotope composition of seawater.

| Seawater | $\delta^{18}O$ (‰) | $\Delta'^{17}O$ (‰) |
|---|---|---|
| Modern world | 0 (e.g., Luz and Barkan, 2010) | −0.005 |
| Ice-free world | −1 (Shackleton and Kennett, 1975) | −0.004 |
| Glacial Maximum | 1 (Schrag et al., 2002) | 0.006 |
| Model result[a] | −0.36 | −0.017 |
| Model result with $F_{sp}$ 25% lower, $F_{cw}$ 25% higher[a] | −1.2 | −0.004 |
| Model result with $F_{sp}$ 40% lower, $F_{cw}$ 75% higher[a] | −1 | −0.004 |

[a] All flux values are from Muehlenbachs (1998).

**Table 5**
Results of the sensitivity test for the mass balance model.

| Input parameters | Sensitivity | |
|---|---|---|
| | $\partial(\delta^{18}O)/\partial$(parameter) | $\partial(\Delta'^{17}O)/\partial$(parameter) |
| $F_{cw}$ | $-6.9\times10^{-14}$‰/kg O yr$^{-1}$ | $9.8\times10^{-16}$‰/kg O yr$^{-1}$ |
| $F_{sp}$ | $7.0\times10^{-14}$‰/kg O yr$^{-1}$ | $-1.1\times10^{-15}$‰/kg O yr$^{-1}$ |
| $F_{sfw}$ | $-1.8\times10^{-13}$‰/kg O yr$^{-1}$ | 0‰/kg O yr$^{-1}$ |
| $F_{cg}$ | $-1.3\times10^{-13}$‰/kg O yr$^{-1}$ | 0‰/kg O yr$^{-1}$ |
| $F_r$ | $-1.3\times10^{-16}$‰/kg O yr$^{-2}$ | 0‰/kg O yr$^{-1}$ |
| Shale, $F_{cw}$ end member | −0.12‰/‰ | 0.003‰/‰ |
| Igneous crust | 0.06‰/‰ | −0.002‰/‰ |
| Metamorphic crust | 0.06‰/‰ | −0.034‰/‰ |
| OC_HT_1, $F_{sp}$ end member | −0.89‰/‰ | −0.012‰/‰ |
| $F_{sfw}$ end member | 0.02‰/‰ | −0.0005‰/‰ |
| Deep sea sediments | 0.00‰/‰ | −0.004‰/‰ |
| Connate water | 0.04‰/‰ | −0.021‰/‰ |

10‰ or more) in the Earth's past (e.g., Jaffrés et al., 2007, and references therein). The mass balance shows that two dominant processes control the composition of seawater: continental weathering ($F_{cw}$) and high-T oceanic crust alteration ($F_{sp}$; Fig. 1). In order to study the effect of variations in $F_{cw}$ and $F_{sp}$, we have varied theses fluxes to see how $\delta^{18}O^{SW}$ and $\Delta'^{17}O^{SW}$ changes. Increasing $F_{cw}$ by a factor of 10decreases the $\delta^{18}O^{SW}$ to −3.5‰; a 100-fold increase results in a steady-state $\delta^{18}O^{SW}$ = −6.2‰. The corresponding $\Delta'^{17}O$ increases to 0.055 and 0.115‰, respectively (Fig. 7A).

The slope of the trajectory on which the changing seawater with varying $F_{cw}$ falls is $\lambda_{cw}$ = 0.5077. Decreasing $F_{sp}$ by a factor of 0.5 decreases the $\delta^{18}O^{SW}$ to −1.5‰ (Fig. 7B). Entire shutting off of $F_{sp}$ results in $\delta^{18}O^{SW}$ = −8‰. The corresponding $\Delta'^{17}O$ increases to 0.005 and 0.135‰, respectively. The slope of the trajectory, on which the changing seawater falls is $\lambda_{sp}$ = 0.5105, which is similar to the slope corresponding to increased $F_{cw}$.

It can now be tested if cherts can have ever have equilibrated with such a low- $\delta^{18}O$ seawater. Levin et al. (2014) published high-precision triple oxygen isotope data on 3 Phanerozoic and 5 Archean chert samples. We display these chert data in the triple oxygen isotope space

**Table 3**
List of input parameters for mass balance model. Fluxes and most $\Delta(\delta^{18}O)$ are from Muehlenbachs (1998).

| Process | Flux (kg O year$^{-1}$) | $\Delta(\delta^{18}O)$ (‰) | $\Delta(\delta^{17}O)$ (‰) |
|---|---|---|---|
| High-temperature alteration oceanic crust ($F_{sp}$) | $18.7\times10^{12}$ ± 10% | $1.3-\delta^{18}O^{sw}$ | $0.631-\delta^{17}O^{sw}$ |
| Low-temperature alteration oceanic crust ($F_{sfw}$) | $2.18\times10^{12}$ ± 10% | $1.16-0.2\times(25+\delta^{18}O^{sw})$ | $0.603-0.2\times(13.037+\delta^{17}O^{sw})$ |
| Continental weathering ($F_{cw}$) | $10.2\times10^{12}$ ± 13% | $0.125\times(-9.1-\delta^{18}O^{sw})+0.125\times(-4.1-\delta^{18}O^{sw})$ | $0.125\times(-4.702-\delta^{17}O^{sw})+0.125\times(-2.065-\delta^{17}O^{sw})$ |
| Continental growth ($F_{cg}$) | $1.53\times10^{12}$ ± 10% | $5.5-(0.9\times5.8)-0.156\times(26+\delta^{18}O^{sw})$ | $2.853-(0.9\times3.013)-0.156\times(13.547+\delta^{17}O^{sw})$ |
| Mantle recycling ($F_r$) | $0.82\times10^{12}$ ± 10% | $-3+\delta^{18}Osw$ | $-1.558+\delta^{17}O^{sw}$ |

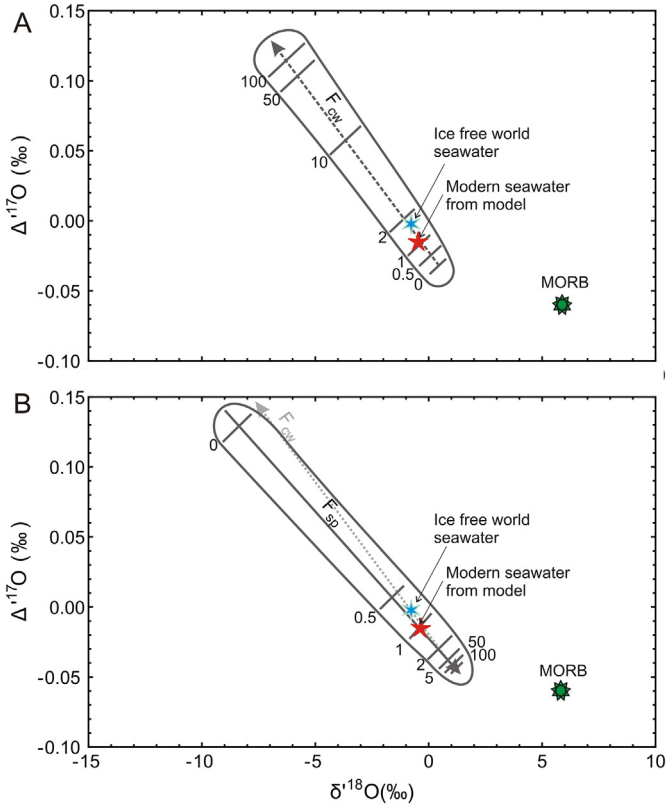


**Fig. 7.** Plots of $\Delta'^{17}O$ vs. $\delta'^{18}O$ showing the effect of varying the modern fluxes for continental weathering ($F_{cw}$) (A) and high-T oceanic crust alteration ($F_{sp}$) (B). Both fluxes have been decreased from 100 times their modern values to 0. The 1σ error interval from the mass balance calculation is indicated. The MORB value is shown by a green complex star (based on values from Pack et al., 2016 and Sharp et al., 2016). (For interpretation of the references to colour in this figure legend, the reader is referred to the web version of this article.)

in Fig. 8 along with silica-water equilibration curves from Sharp et al. (2016) and the seawater evolution trend from this study. We also consider closed-system diagenetic alteration with different T, pore water compositions, and water/rock ratios adopting the model by Taylor (1978), Eq. (9) and Eq. (10)in our study; see also Sharp et al., 2018).

$$\delta^{18}_{bulk} = \underbrace{X_w \cdot \delta^{18}_{w,i}}_{\text{meteoric water or mixture of meteroic water and seawater}} + \underbrace{(1 - X_w)\cdot\delta^{18}_{ch,i}}_{\text{on the silica–water equilibrium curve}} \quad (9)$$

$$\delta^{18}_{bulk} = X_w \cdot \delta^{18}_{w,\,f} + (1 - X_w)\cdot\delta^{18}_{ch,\,f} \quad (10)$$

where w = water, ch = chert, i = initial composition, f = final composition, $X_w$ = mole fraction of water in the closed water-chert system. Equations for $^{17}O$ are shown below (Eq. (11) to Eq. (14)). In addition to these we have used Eq. (11) to Eq. (14)for the triple isotope calculations.

$$\delta^{17}_{bulk} = X_w \cdot \delta^{17}_{w,\,f} + (1 - X_w)\cdot\delta^{17}_{ch,\,f} \quad (11)$$

$$\delta^{17}_{bulk} = X_w \cdot \delta^{17}_{w,\,f} + (1 - X_w)\cdot\delta^{17}_{ch,\,f} \quad (12)$$

$$\frac{\delta^{18}_{ch,f} + 1000}{\delta^{18}_{w,f} + 1000} = \alpha^{18}_{SiO_2-w}(T) \quad (13)$$

$$\frac{\delta^{17}_{ch,f} + 1000}{\delta^{17}_{w,f} + 1000} = \alpha^{17}_{SiO_2-w} = (\alpha^{18}_{SiO_2-w})^{\theta_{SiO_2-w}(T)} \quad (14)$$

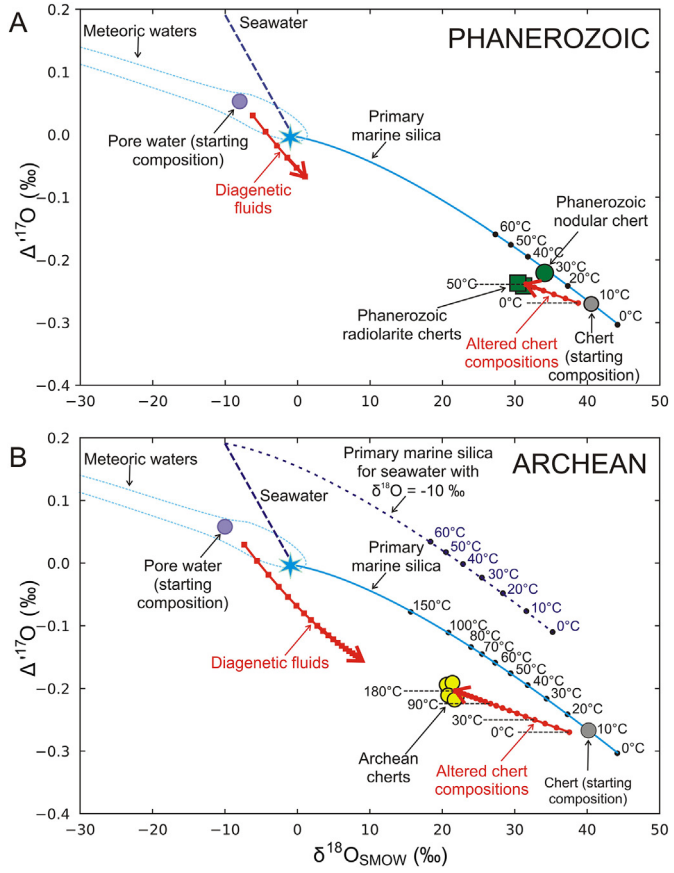


**Fig. 8.** Plot of Phanerozoic (A) and Archean (B) chert data from Levin et al. (2014; normalized to $\Delta'^{17}O$ for San Carlos Olivine = −0.060‰, based on values from Pack et al., 2016 and Sharp et al., 2016). A) The Phanerozoic nodular chert (solid green circle) is explained by early diagenetic equilibration with seawater at 30 °C or diagenetic exchange with meteoric water or a mixture between meteoric water and seawater at high water/rock ratios (alteration trend not displayed). The composition of the Phanerozoic radiolaritic chert (solid green squares) is explained by precipitation of marine silica at ~8 °C (gray circle on equilibrium curve) followed by diagenetic modification with meteoric water ($\delta^{18}O$ = −6 ‰) at 50 °C and a water/rock ratio of ~1 (using Eqs. (9) to (14)). B) The Archean cherts (solid yellow circles) falls off the seawater equilibration curve and is clearly not explained by equilibration with modern-like seawater at high T (hot oceans or marine hydrothermal systems). Also seawater with lower $\delta^{18}O$ (dashed blue line, slope λ = 0.51, from mass balance, this study) does not explain the observed composition of the chert. Precipitation of primary silica from an ocean with a similar composition than today (ice-free) at 11 °C (solid gray circle) followed by diagenesis with a meteoric fluid ($\delta^{18}O$ = −10‰) at ~180 °C and a water/rock ratio of 1, however, would explain the observed chert composition. For both panels alteration models have been drawn in red. The diagenetic fluids (red squares) and the altered chert (red circles) curves have been derived for a water/rock ratio of 1, based on equations given by Taylor (1978) and using the silica-water equilibration data from Sharp et al. (2018) (Eqs. (9) to (14)). As diagenesis proceeds with temperature increase the original compositions of both the chert and the diagenetic fluid is modified. For a water/rock ratio of 1 the rock and water oxygen isotope compositions gradually come closer to each other due to lower fractionations at higher temperatures. (For interpretation of the references to colour in this figure legend, the reader is referred to the web version of this article.)

For the Phanerozoic nodular chert (Fig. 8A; solid green circle), early diagenetic equilibration with modern (ice-free world) seawater at 30 °C readily explains the observed isotope composition. For nodular cherts, diagenetic alteration by exchange with a mixture between meteoric and seawater has been suggested (Knauth, 1979). Such a scenario is also in agreement with the observed data but requires a high water/rock ratio.

The composition of the Phanerozoic radiolaritic chert (Fig. 8A) falls off the seawater equilibrium curve and hence cannot be explained by equilibration with seawater at any T. Instead, post-depositional diagenetic exchange with typical meteoric water ($\delta^{18}O \approx -6‰$) at 50 °C explains the observed isotope composition. The model of Taylor (1978), when applied to 3-O-isotopes, allows back-extrapolation to the composition of the original soft sediment, which has been in equilibrium with seawater (Dodd and Sharp, 2010). Here, back-extrapolation to silica in equilibrium with seawater at ~8 °C is one possible explanation for the observed chert composition.

The Archean cherts analyzed by Levin et al. (2014; Fig. 8B) clearly fall off the seawater equilibration trend and hence cannot be explained by equilibration with seawater at high T (open ocean T or in marine hydrothermal systems; Knauth and Epstein, 1976; Knauth and Lowe, 1978, 2003; Shemesh et al., 1983, 1988; Karhu and Epstein, 1986; Jean-Baptiste et al., 1997; Muehlenbachs, 1998; Knauth, 2005; Robert and Chaussidon, 2006; Blake et al., 2010; Marin et al., 2010; Tartèse et al., 2017; Garcia et al., 2017). Nor is a low-$\delta^{18}O$ hydrosphere (Perry, 1967; Veizer et al., 1999; Wallmann, 2001; Kasting et al., 2006; Jaffrés et al., 2007; Shields, 2007) an explanation for the low $\delta^{18}O$ of the cherts. In such case, $\Delta'^{17}O$ values must be much higher than the ~ −0.210‰ observed by Levin et al. (2014) as the seawater evolution trend has a slope of ~0.51 (Fig. 7). For hot Archean oceans the cherts must have $\Delta'^{17}O$ close to −0.100‰; for a low $\delta^{18}O$ ocean the $\Delta'^{17}O$ of the cherts should be around −0.075‰ (at ~10 °C equilibration temperature). The reported values are > 0.1‰ lower than these numbers and therefore do not qualify for equilibrium with hot or low $\delta^{18}O$ seawater.

Instead, diagenetic modification of the analyzed cherts (as suggested by Degens and Epstein, 1962) at ~180 °C with meteoric water ($\delta^{18}O = -10‰$) and a water/rock ratio of ~1 explains the observed isotope composition (Fig. 8B) of the cherts. The putative silica precursor could have been in equilibration with seawater at $T = 11$ °C. This interpretation of the triple oxygen isotope data supports the idea of a cool Archean with bottom temperatures < ~30 °C. It is possible to arrive at this altered chert composition from starting compositions different to those described here. But the low $\Delta'^{17}O$ of the final rock still points to cool (< 30 °C) formation temperatures.

In order to draw a more comprehensive picture of the conditions during the Archean, however, clearly more data are necessary than presented here; instead the application to published chert data shall demonstrate that triple oxygen isotope data provide important additional information when compared to traditional $\delta^{18}O$ studies only.

## 6. Conclusions

We presented a triple oxygen isotope mass balance model for the Earth's hydrosphere. For modern oceans, the mass balance suggests that the ratio of continental weathering to high-T seafloor alteration may be 25% higher than previously assumed. Parameters such as seafloor spreading rates and depth of high-T alteration in the oceanic crust may need revision. Phanerozoic cherts are explained by precipitation from seawater followed by diagenesis with involvement of meteoric water at moderate temperatures. Published Archean cherts cannot be explained by high T or by low-$\delta^{18}O$ oceans. Instead, post-depositional alteration at elevated T likely altered the original chemical sedimentary signature. Back-extrapolation of the alteration trend suggest that the protolith of the studied Archean cherts may have once equilibrated with modern-like ocean water at low T; furthermore, supporting a cool Archean.

## Acknowledgements

This study was funded by the Deutsche Forschungsgemeinschaft (DFG; PA 909/14-1, PI: AP) within the Priority Program SPP 1833 “Building a habitable Earth”. Wolfgang Bach (University of Bremen) is thanked for making available the drill core samples analyzed in this study. Comments and suggestions by two anonymous reviewers led to improvement of the manuscript. The editorial handling by Michael Böttcher is appreciated.

## References

Affolter, S., Häuselmann, A.D., Fleitmann, D., Häuselmann, P., Leuenberger, M., 2015. Triple isotope (δD, $\delta^{17}O$, $\delta^{18}O$) study on precipitation, drip water and speleothem fluid inclusions for a Western Central European cave (NW Switzerland). Quat. Sci. Rev. 127, 73–89.

Alt, J.C., Muehlenbachs, K., Honnorez, J., 1986. An oxygen isotopic profile through the upper kilometer of the oceanic crust, DSDP Hole 504B. Earth Planet. Sci. Lett. 80, 217–229.

Alt, J.C., Laverne, C., Vanko, D.A., Tartarotti, P., Teagle, D.A., Bach, W., Zuleger, E., Erzinger, J., Honnorez, J., Philippe, P.A., Becker, K., Salisbury, M.H., Wilkens, R.H., Becker, K.H.S.M., 1996. Hydrothermal alteration of a section of upper oceanic crust in the eastern equatorial Pacific: a synthesis of results from Site 504 (DSDP Legs 69, 70, and 83, and ODP Legs 111, 137, 140 and 148). Proc. Ocean Drill. Program Sci. Results 148, 417–434.

Bach, W., Peucker-Ehrenbrink, B., Hart, S.R., Blusztajn, J.S., 2003. Geochemistry of hydrothermally altered oceanic crust: DSDP/ODP Hole 504B - implications for seawater - crust exchange budgets and Sr- and Pb-isotopic evolution of the mantle. Geochem. Geophys. Geosyst. 4.

Banner, J.L., Hanson, G.N., 1990. Calculation of simultaneous isotopic and trace element variations during water-rock interaction with applications to carbonate diagenesis. Geochim. Cosmochim. Acta 54, 3123–3137.

Barkan, E., Luz, B., 2005. High precision measurements of $^{17}O/^{16}O$ and $^{18}O/^{16}O$ ratios in $H_2O$. Rapid Commun. Mass Spectrom. 19, 3737–3742.

Bindeman, I.N., Zakharov, D.O., Palandri, J., Greber, N.D., Dauphas, N., Retallack, G.J., Hofmann, Lackey, J.S., Bekker, A., 2018. Rapid emergence of subaerial landmasses and onset of a modern hydrologic cycle 2.5 billion years ago. Nature 557, 545–549.

Blake, R.E., Chang, S.J., Lepland, A., 2010. Phosphate oxygen isotopic evidence for a temperate and biologically active Archaean ocean. Nature 464, 1029–1032.

Bottjer, D.J., Droser, M.L., Sheehan, P.M., McGhee, G.R., 2001. The ecological architecture of major events in the Phanerozoic history of marine invertebrate life. In: Warren, A., Bottjer, D.J. (Eds.), Evolutionary Paleoecology: The Ecological Context of Macroevolutionary Change. Columbia University Press, New York, pp. 35–61.

Cao, X., Liu, Y., 2011. Equilibrium mass-dependent fractionation relationships for triple oxygen isotopes. Geochim. Cosmochim. Acta 75, 7435–7445.

Clayton, R.N., Mayeda, T.K., 1963. The use of bromine pentafluoride in the extraction of oxygen from oxides and silicates for isotopic analysis. Geochim. Cosmochim. Acta 27, 43–52.

Degens, E.T., Epstein, S., 1962. Relationship between $O^{18}/O^{16}$ ratios in coexisting carbonates, cherts, and diatomites: geological notes. AAPG Bull. 46, 534–542.

Di Rocco, T., Pack, A., 2015. Triple oxygen isotope exchange between chondrule melt and water vapor: an experimental study. Geochim. Cosmochim. Acta 164, 17–34.

Dodd, J.P., Sharp, Z.D., 2010. A laser fluorination method for oxygen isotope analysis of biogenic silica and a new oxygen isotope calibration of modern diatoms in freshwater environments. Geochim. Cosmochim. Acta 74, 1381–1390.

Expedition 336 Scientists, 2012. Expedition 336 summary. In: Edwards, K.J., Bach, W., Klaus, A., the Expedition 336 Scientists (Eds.), Proc. IODP, 336: Tokyo (Integrated Ocean Drilling Program Management International, Inc.).

Fiebig, J., Wiechert, U., Rumble III, D., Hoefs, J., 1999. High-precision in situ oxygen isotope analysis of quartz using an ArF laser. Geochim. Cosmochim. Acta 63, 687–702.

Garcia, A.K., Schopf, J.W., Yokobori, S., Akanuma, S., Yamagishi, A., 2017. Reconstructed enzymes suggest hot early Earth. Proc. Natl. Acad. Sci. 114, 4619–4624.

Herwartz, D., Pack, A., Krylov, D., Xiao, Y., Muehlenbachs, K., Sengupta, S., Di Rocco, T., 2015. Revealing the climate of snowball Earth from $\Delta^{17}O$ systematics of hydrothermal rocks. Proc. Natl. Acad. Sci. 112, 5337–5341.

Jaffrés, J.B.D., Shields, G.A., Wallmann, K., 2007. The oxygen isotope evolution of seawater: a critical review of a long-standing controversy and an improved geological water cycle model for the past 3.4 billion years. Earth Sci. Rev. 83, 83–122.

Jean-Baptiste, P., Charlou, J.L., Stievenard, M., 1997. Oxygen isotope study of mid-ocean ridge hydrothermal fluids: Implication for the oxygen-18 budget of the oceans. Geochim. Cosmochim. Acta 61, 2669–2677.

Karhu, J., Epstein, S., 1986. The implication of the oxygen isotope records in coexisting cherts and phosphates. Geochim. Cosmochim. Acta 50, 1745–1756.

Kasting, J.F., Howard, M.T., Wallmann, K., Veizer, J., Shields, G., Jaffrés, J., 2006. Paleoclimates, ocean depth, and the oxygen isotopic composition of seawater. Earth Planet. Sci. Lett. 252, 82–93.

Kawahata, H., Kusakabe, M., Kikuchi, Y., 1987. Strontium, oxygen, and hydrogen isotope geochemistry of hydrothermally altered and weathered rocks in DSDP Hole 504B, Costa Rica Rift. Earth Planet. Sci. Lett. 85, 343–355.

Knauth, L.P., 2005. Temperature and salinity history of the Precambrian ocean: implications for the course of microbial evolution. Palaeogeogr. Palaeoclimatol. Palaeoecol. 219, 53–69.

Knauth, L.P., 1979. A model for the origin of chert in limestone. Geology 7, 274–277.

Knauth, L.P., Epstein, S., 1976. Hydrogen and oxygen isotope ratios in nodular and bedded cherts. Geochim. Cosmochim. Acta 40, 1095–1108.

Knauth, L.P., Lowe, D.R., 1978. Oxygen isotope geochemistry of cherts from the Onverwacht Group (3.4 billion years), Transvaal, South Africa, with implications for secular variations in the isotopic composition of cherts. Earth Planet. Sci. Lett. 41, 209–222.

Knauth, L.P., Lowe, D.R., 2003. High Archean climatic temperature inferred from oxygen isotope geochemistry of cherts in the 3.5 Ga Swaziland Supergroup, South Africa. Bull. Geol. Soc. Am. 115, 566–580.
Landais, A., Barkan, E., Luz, B., 2008. Record of $\delta^{18}O$ and $^{17}O$-excess in ice from Vostok Antarctica during the last 150,000 years. Geophys. Res. Lett. 35.
Landais, A., Steen-Larsen, H.C., Guillevic, M., Masson-Delmotte, V., Vinther, B., Winkler, R., 2012a. Triple isotopic composition of oxygen in surface snow and water vapor at NEEM (Greenland). Geochim. Cosmochim. Acta 77, 304–316.
Landais, A., Ekaykin, A., Barkan, E., Winkler, R., Luz, B., 2012b. Seasonal variations of $^{17}O$-excess and d-excess in snow precipitation at Vostok station, East Antarctica. J. Glaciol. 58, 725–733.
Levin, N.E., Raub, T.D., Dauphas, N., Eiler, J.M., 2014. Triple oxygen isotope variations in sedimentary rocks. Geochim. Cosmochim. Acta 139, 173–189.
Li, S., Levin, N.E., Chesson, L.A., 2015. Continental scale variation in $^{17}O$-excess of meteoric waters in the United States. Geochim. Cosmochim. Acta 164, 110–126.
Longinelli, A., Nuti, S., 1968. Oxygen isotopic composition of phosphorites from marine formations. Earth Planet. Sci. Lett. 5, 13–16.
Luz, B., Barkan, E., 2010. Variations of $^{17}O/^{16}O$ and $^{18}O/^{16}O$ in meteoric waters. Geochim. Cosmochim. Acta 74, 6276–6286.
Luz, B., Barkan, E., 2011. The isotopic composition of atmospheric oxygen. Glob. Biogeochem. Cycles 25, 1–14.
Marin, J., Chaussidon, M., Robert, F., 2010. Microscale oxygen isotope variations in 1.9 Ga Gunflint cherts: assessments of diagenesis effects and implications for oceanic paleotemperature reconstructions. Geochim. Cosmochim. Acta 74, 116–130.
Matsuhisa, Y., Goldsmith, J.R., Clayton, R.N., 1978. Mechanisms of hydrothermal crystallization of quartz at 250 °C and 15 kbar. Geochim. Cosmochim. Acta 42, 173–182.
McKinney, C.R., McCrea, J.M., Epstein, S., Allen, H.A., Urey, H.C., 1950. Improvements in mass spectrometers for the measurement of small differences in isotope abundance ratios. Rev. Sci. Instrum. 21, 724–730.
Muehlenbachs, 1998. The oxygen isotopic composition of the oceans, sediments and the seafloor. Chem. Geol. 145, 263–273.
Muehlenbachs, K., Clayton, R.N., 1972. Oxygen isotope geochemistry of submarine greenstones. Can. J. Earth Sci. 95, 471–478.
Muehlenbachs, K., Clayton, R.N., 1976. Oxygen isotope composition of the oceanic crust and its bearing on seawater. J. Geophys. Res. 81, 4365.
Nutman, A.P., McGregor, V., Friend, C.R.L., 1996. The Itsaq Gneiss Complex of southern West Greenland; the world's most extensive record of early crustal evolution. Precambrian Res. 78, 1–39.
Nutman, A.P., Mojzsis, S.J., Friend, C.R.L., 1997. Recognition of ≥3850 Ma water-lain sediments in West Greenland and their significance for the early Archaean Earth. Geochim. Cosmochim. Acta 61, 2475–2484.
Orcutt, B.N., Wheat, C.G., Rouxel, O., Hulme, S., Edwards, K.J., Bach, W., 2013. Oxygen consumption rates in subseafloor basaltic crust derived from a reaction transport model. Nat. Commun. 4, 2539.
Pack, A., Herwartz, D., 2014. The triple oxygen isotope composition of the Earth mantle and understanding $\Delta^{17}O$ variations in terrestrial rocks and minerals. Earth Planet. Sci. Lett. 390, 138–145.
Pack, A., Herwartz, D., 2015. Observation and interpretation of $\Delta^{17}O$ variations in terrestrial rocks – response to the comment by Miller et al. on the paper by Pack & Herwartz (2014). Earth Planet. Sci. Lett. 418, 184–186.
Pack, A., Tanaka, R., Hering, M., Sengupta, S., Peters, S., Nakamura, E., 2016. The oxygen isotope composition of San Carlos olivine on the VSMOW2-SLAP2 scale. Rapid Commun. Mass Spectrom. 30, 1495–1504.
Peck, W.H., Valley, J.W., Wilde, S.A., Graham, C.M., 2001. Oxygen isotope ratios and rare Earth elements in 3.3 to 4.4 Ga zircons: ion microprobe evidence for high $\delta^{18}O$ continental crust and oceans in the early Archean. Geochim. Cosmochim. Acta 65, 4215–4229.
Perry, E.C., 1967. The oxygen isotope chemistry of ancient cherts. Earth Planet. Sci. Lett. 3, 62–66.
Robert, F., Chaussidon, M., 2006. A palaeotemperature curve for the Precambrian oceans based on silicon isotopes in cherts. Nature 443, 969–972.
Rumble, D., Miller, M.F., Franchi, I.A., Greenwood, R.C., 2007. Oxygen three-isotope fractionation lines in terrestrial silicate minerals: an inter-laboratory comparison of hydrothermal quartz and eclogitic garnet. Geochim. Cosmochim. Acta 71, 3592–3600.
Schrag, D.P., Adkins, J.F., McIntyre, K., Alexander, J.L., Hodell, D.A., Charles, C.D., McManus, J.F., 2002. The oxygen isotopic composition of seawater during the Last Glacial Maximum. Quat. Sci. Rev. 21, 331–342.
Shackleton, N.J., Kennett, J.P., 1975. Paleotemperature history of the Cenozoic and the initiation of Antarctic glaciation; oxygen and carbon isotope analyses in DSDP sites 277, 279 and 281. Initial Rep. Deep Sea Drill. Proj. 29, 743–755.
Sharp, Z.D., 1990. A laser-based microanalytical method for the in situ determination of oxygen isotope ratios of silicates and oxides. Geochim. Cosmochim. Acta 54, 1353–1357.
Sharp, Z.D., Gibbons, J.A., Maltsev, O., Atudorei, V., Pack, A., Sengupta, S., Shock, E.L., Knauth, L.P., 2016. A calibration of the triple oxygen isotope fractionation in the $SiO_2$-$H_2O$ system and applications to natural samples. Geochim. Cosmochim. Acta 186, 105–119.
Sharp, Z.D., Wostbrock, J.A.G., Pack, A., 2018. Mass-dependent triple oxygen isotope variations in terrestrial materials. Geochem. Perspect. Lett. 7, 27–31.
Shemesh, A., Kolodny, Y., Luz, B., 1983. Oxygen isotope variations in phosphate of biogenic apatites, II. Phosphorite rocks. Earth Planet. Sci. Lett. 64, 405–416.
Shemesh, A., Kolodny, Y., Luz, B., 1988. Isotope geochemistry of oxygen and carbon in phosphate and carbonate of phosphorite francolite. Geochim. Cosmochim. Acta 52, 2565–2572.
Sheppard, S.M.F., Gilg, H.A., 1996. Stable isotope geochemistry of clay minerals. Clay Miner. 31, 1–24.
Shields, G.A., 2007. Chapter 7.6 the marine carbonate and chert isotope records and their implications for tectonics, life and climate on the early Earth. Dev. Precambrian Geol. 15, 971–983.
Silverman, S.R., 1951. The isotope geology of oxygen. Geochim. Cosmochim. Acta 39, 569–584.
Surma, J., Assonov, S., Bolourchi, M.J., Staubwasser, M., 2015. Triple oxygen isotope signatures in evaporated water bodies from the Sistan Oasis, Iran. Geophys. Res. Lett. 42, 8456–8462.
Tartèse, R., Chaussidon, M., Gurenko, A., Delarue, F., Robert, F., 2017. Warm Archaean oceans reconstructed from oxygen isotope composition of early-life remnants. Geochem. Perspect. Lett. 3, 55–65.
Taylor, H.P., 1978. Oxygen and hydrogen isotope studies of plutonic granitic rocks. Earth Planet. Sci. Lett. 38, 177–210.
Veizer, J., Hoefs, J., 1976. The nature of $O^{18}/O^{16}$ and $C^{13}/C^{12}$ secular trends in sedimentary carbonate rocks. Geochim. Cosmochim. Acta 40, 1387–1395.
Veizer, J., Ala, D., Azmy, K., Bruckschen, P., Buhl, D., Bruhn, F., Carden, G.A.F., Diener, A., Ebneth, S., Godderis, Y., Jasper, T., Korte, C., Pawellek, F., Podlaha, O.G., Strauss, H., 1999. $^{87}Sr$ $^{86}Sr$, $\delta^{13}C$ and $\delta^{18}O$ evolution of Phanerozoic seawater. Chem. Geol. 161, 59–88.
Villinger, H., 2014. Borehole Microbial Observatory Science in Basaltic Ocean Crust: The North Pond Area on the Western Mid-Atlantic Ridge flank at 23° N MICROB II - Cruise MSM37 –March 22 – April 21, 2014 – Las Palmas (Spain) – Cadiz (Spain). MARIA S. MERIAN-Berichte, MSM37, 42 pp.. DFG-Senatskommission für Ozeanographie.
Wallmann, K., 2001. The geological water cycle and the evolution of marine $\delta^{18}O$ values. Geochim. Cosmochim. Acta 65, 2469–2485.
Wilde, S.A., Valley, J.W., Peck, W.H., Graham, C.M., 2001. Evidence from detrital zircons for the existence of continental crust and oceans on the Earth 4.4 Gyr ago. Nature 409, 175–178.
Young, E.D., Galy, A., Nagahara, H., 2002. Kinetic and equilibrium mass-dependent isotope fractionation laws in nature and their geochemical and cosmochemical significance. Geochim. Cosmochim. Acta 66, 1095–1104.